THE UNIVERSITY of EDINBURGH

Edinburgh Research Explorer

Relating source-receiver interferometry to an inverse-scattering series to derive a new method to estimate internal multiples

Citation for published version:
Löer, K, Curtis, A & Angelo Meles, G 2016, 'Relating source-receiver interferometry to an inverse-scattering series to derive a new method to estimate internal multiples' Geophysics, vol. 81, no. 3, pp. Q27-Q40. DOI: 10.1190/geo2015-0330.1

Digital Object Identifier (DOI):
10.1190/geo2015-0330.1

Link:
Link to publication record in Edinburgh Research Explorer

Document Version:
Publisher's PDF, also known as Version of record

Published In:
Geophysics

Publisher Rights Statement:
© 2016 Society of Exploration Geophysicists. All rights reserved

General rights
Copyright for the publications made accessible via the Edinburgh Research Explorer is retained by the author(s) and / or other copyright owners and it is a condition of accessing these publications that users recognise and abide by the legal requirements associated with these rights.

Take down policy
The University of Edinburgh has made every reasonable effort to ensure that Edinburgh Research Explorer content complies with UK legislation. If you believe that the public display of this file breaches copyright please contact openaccess@ed.ac.uk providing details, and we will remove access to the work immediately and investigate your claim.

Download date: 05. Apr. 2019

GEOPHYSICS, VOL. 81, NO. 3 (MAY-JUNE 2016); P. Q27–Q40, 9 FIGS.
10.1190/GEO2015-0330.1

Downloaded 04/08/16 to 129.215.249.201. Redistribution subject to SEG license or copyright; see Terms of Use at http://library.seg.org/

Relating source-receiver interferometry to an inverse-scattering series to derive a new method to estimate internal multiples

Katrin Löer[1], Andrew Curtis[1], and Giovanni Angelo Meles[1]

ABSTRACT

We have evaluated an explicit relationship between the representations of internal multiples by source-receiver interferometry and an inverse-scattering series. This provides a new insight into the interaction of different terms in each of these internal multiple prediction equations and explains why amplitudes of estimated multiples are typically incorrect. A downside of the existing representations is that their computational cost is extremely high, which can be a precluding factor especially in 3D applications. Using our insight from source-receiver interferometry, we have developed an alternative, computationally more efficient way to predict internal multiples. The new formula is based on crosscorrelation and convolution: two operations that are computationally cheap and routinely used in interferometric methods. We have compared the results of the standard and the alternative formulas qualitatively in terms of the constructed wavefields and quantitatively in terms of the computational cost using examples from a synthetic data set.

INTRODUCTION

Interferometry refers to a set of methods that allow us to synthesize Green's functions between pairs of receivers (interreceiver interferometry; Wapenaar, 2004; van Manen et al., 2005, 2006; Wapenaar and Fokkema, 2006), pairs of sources (intersource interferometry; Hong and Menke, 2006; Curtis et al., 2009), or a source and a receiver (source-receiver interferometry [SRI]; Curtis and Halliday, 2010) by means of crosscorrelation, convolution, or deconvolution (e.g., Vasconcelos and Snieder, 2008) of wavefields. The latter of the three methods, SRI, has been subject to increasing interest due to its close relationship to seismic imaging methods (Halliday and Curtis, 2010) and the new perspective it provides on nonlinear imaging schemes and so-called extended images (Vasconcelos et al., 2010; Fleury and Vasconcelos, 2012; Ravasi and Curtis, 2013; Ravasi et al., 2014). Other applications of SRI include ground-roll removal in land-based exploration seismology (Duguid et al., 2011), construction of underside reflections from borehole recordings (Poliannikov, 2011), retrospectively observing seismograms from old earthquakes in seismology (Curtis et al., 2012; Entwistle et al., 2015), suppression of nonphysical reflections in standard interferometry (King and Curtis, 2012), and prediction of multiply diffracted events and identification of scattering paths (Meles and Curtis, 2014; Löer et al., 2015). We focus on this last application and show that by considering multiple reflected scattering paths, a new method is obtained to predict internal multiples in reflection seismic data.

Although surface-related multiples cause major problems in marine seismic data, internal multiples (i.e., interbed multiples generated between subsurface stratal interfaces) still affect marine and land data in the presence of strong reflectors, such as the water bottom, and the top and bottom of salt or basalt layers. Though there have been attempts to use multiply scattered waves in seismic imaging (e.g., Jiang et al., 2007; Malcolm et al., 2009; Fleury, 2013), most migration schemes rely on a single-scattering assumption and therefore require surface-related and internal multiples to be removed from the data prior to migration.

Suppression of surface-related multiples has been addressed successfully by a few methods (Verschuur, 2013), whereas relatively few methods exist that identify and attenuate internal multiples. Methods that rely on move-out discrimination, for example, in the Radon domain (Hampson, 1986), tend to fail for internal multiples because their moveout velocities are often similar to those of primaries. Berkhout and Verschuur (1997) propose a layer-related internal multiple elimination scheme (based on surface-related multiple elimination; Verschuur et al., 1992) that downward extrapolates shot records to a virtual acquisition surface and eliminates all multiples generated by that surface. This method, however, requires a velocity

Manuscript received by the Editor 18 June 2015; revised manuscript received 21 October 2015; published online 04 April 2016.
[1]The University of Edinburgh, School of GeoSciences, Grant Institute, The King's Buildings, Edinburgh, UK. E-mail: katrin.loer@posteo.de; andrew.curtis@ed.ac.uk; gmeles@ed.ac.uk.
© 2016 Society of Exploration Geophysicists. All rights reserved.

Downloaded 04/08/16 to 129.215.249.201. Redistribution subject to SEG license or copyright; see Terms of Use at http://library.seg.org/

model to create the redatumed data. Jakubowicz (1998) suggests a data-driven approach based on the work of Keydar et al. (1997) that combines three primary reflections to predict a first-order multiple. However, the primary reflection from the interface generating the interbed multiple needs to be identified and isolated from the recorded data, which can be difficult. Other schemes based on the same idea are proposed by Hung and Wang (2012) and Behura and Forghani (2012). Recently, Meles et al. (2014) propose a scheme to estimate multiples based on Marchenko imaging and interferometry that requires autofocusing of wavefields, a relatively novel technique in seismics. The method has been applied successfully to synthetic data sets but still needs to be tested on real data. Another data-driven algorithm that predicts all internal multiples at once is first presented by Araujo et al. (1994) and is described in detail by Weglein et al. (1997, 2003). Traveltimes of internal multiples are predicted using a subseries of an inverse-scattering series (ISS) derived from the Lippmann-Schwinger equation (Lippmann and Schwinger, 1950). This method is promising but has the downside that it is computationally expensive. Malcolm and De Hoop (2005) and Malcolm et al. (2007) suggest similar but significantly faster algorithms; however, they require an estimate of a velocity model down to the shallowest reflector involved in multiple generation.

We show explicitly for wave propagation in a 1D medium (a medium that varies only in one dimension) and a collocated source and receiver that the SRI equation to estimate internal multiples is in fact equivalent to the internal-multiple attenuation formula derived from the ISS (Weglein et al., 1997). We provide a concise derivation of both equations and demonstrate their equivalence by making use of a representation of Weglein's formula provided by ten Kroode (2002). Finally, an alternative representation of the same equation based on crosscorrelation and convolution is presented, which provides a more efficient way to compute traveltimes of internal multiples and which decreases computational cost by many orders of magnitude. We use a synthetic data set obtained from a 1D velocity and density model, estimate internal multiples using the standard and the alternative formula, and compare the results qualitatively and quantitatively.

THEORY

We begin by revising the derivation of internal multiples based on an ISS as provided by Weglein et al. (1997), and then we derive the same equation starting from SRI and present an alternative formula based on crosscorrelation and convolution, two operations that are computationally cheap and routinely used in interferometric methods.

An equation for internal multiples derived from an ISS

Starting with an introduction to forward-scattering theory, we examine the third-order scattering term of the Lippmann-Schwinger equation and show that under certain conditions and with the aid of an ISS, this term provides an estimate of internal multiples.

Forward-scattering theory

In a scattering medium, the response to an impulsive source, the so-called Green's function $\mathbf{G}$, can be written as the sum of an unperturbed component $\mathbf{G}_0$ that propagates in a background or reference medium and a perturbed component $\mathbf{G}_S$ that interacts with added scattering perturbations to the medium:

$$\mathbf{G} = \mathbf{G}_0 + \mathbf{G}_S, \tag{1}$$

where the Green's functions $\mathbf{G}$, $\mathbf{G}_0$, and $\mathbf{G}_S$ are third-order tensors with elements $G(\mathbf{x}_j, \mathbf{x}_i, \omega)$, $G_0(\mathbf{x}_j, \mathbf{x}_i, \omega)$, and $G_S(\mathbf{x}_j, \mathbf{x}_i, \omega)$, respectively, where $G(\mathbf{x}_j, \mathbf{x}_i, \omega)$ propagates from spatial location $\mathbf{x}_i$ to $\mathbf{x}_j$ and ω represents different temporal angular frequencies. Wave propagation between a source at $\mathbf{x}_s$ and a receiver at $\mathbf{x}_r$ in the actual and the reference medium is described by the differential equations:

$$\begin{aligned} \mathbf{L}G &= -\delta(\mathbf{x}_r - \mathbf{x}_s) \\ \mathbf{L}_0 G_0 &= -\delta(\mathbf{x}_r - \mathbf{x}_s) \end{aligned} \tag{2}$$

with the differential operators $\mathbf{L} = (\omega^2/\kappa(\mathbf{x})) + \nabla \times (1/\rho(\mathbf{x})\nabla)$ and $\mathbf{L}_0 = (\omega^2/\kappa_0(\mathbf{x})) + \nabla \times (1/\rho_0(\mathbf{x})\nabla)$, where κ and κ_0 as well as ρ and ρ_0 are the actual and the reference bulk modulus and density of the medium, respectively. The perturbed component $\mathbf{G}_S$ is called the scattered field and is the part that carries information about the perturbations to the medium that can be diffractors or reflectors in general. The three Green's functions in equation 1 are related by the Lippmann-Schwinger equation, which in the frequency domain is

$$\mathbf{G}_S = \mathbf{G}_0 \mathbf{V} \mathbf{G}. \tag{3}$$

Here, $\mathbf{V}$ is the perturbation operator defined as the difference between the two differential operators; i.e., $\mathbf{V} = \mathbf{L} - \mathbf{L}_0$. When the problem is discretized, $\mathbf{V}$ is a diagonal matrix in which the diagonal entries are nonzero if $\kappa(\mathbf{x}) \neq \kappa_0(\mathbf{x})$ and/or $\rho(\mathbf{x}) \neq \rho_0(\mathbf{x})$.

Substituting equation 1 into equation 3, and equation 3 into itself repeatedly, the Lippmann-Schwinger equation can be expanded into an infinite series of terms of increasing scattering order according to

$$\begin{aligned} \mathbf{D} &= \mathbf{G}_0\mathbf{V}\mathbf{G}_0 + \mathbf{G}_0\mathbf{V}\mathbf{G}_0\mathbf{V}\mathbf{G}_0 + \mathbf{G}_0\mathbf{V}\mathbf{G}_0\mathbf{V}\mathbf{G}_0\mathbf{V}\mathbf{G}_0 + \ldots \\ &= \mathbf{D}_1 + \mathbf{D}_2 + \mathbf{D}_3 + \ldots, \end{aligned} \tag{4}$$

where $\mathbf{D}_i$ is the ith term in the scattering series. In equation 4, the scattered field on the left side has been replaced by the data $\mathbf{D}$, which (after source signature deconvolution and subtraction of the reference field $\mathbf{G}_0$) we assume is equivalent to the scattered field at the measurement surface. The first term on the right side of equation 4 accounts for first-order scattering and is also known as the single scattering or Born approximation (Born and Wolf, 1999) and is also referred to as the primary wavefield. Our goal is to predict internal multiples, so we focus on the third term that describes third-order scattering as depicted in Figure 1a for a medium with individual point scatterers. Figure 1a shows a special case of third-order scattering, which was chosen deliberately because it resembles the geometry of a typical internal multiple in a horizontally layered reflecting medium (Figure 1b). It satisfies the so-called lower-higher-lower (LHL) condition, which ensures that the first scatterer $\mathbf{x}_1 = (x_1, z_1)$ and the last scatterer $\mathbf{x}_3 = (x_3, z_3)$ are located below the second scatterer $\mathbf{x}_2 = (x_2, z_2)$, expressed as

$$\begin{aligned} z_1 &> z_2 \\ z_3 &> z_2. \end{aligned} \tag{5}$$

Under the LHL condition, the third-order scattering term $\mathbf{G}_0\mathbf{V}\mathbf{G}_0\mathbf{V}\mathbf{G}_0\mathbf{V}\mathbf{G}_0$ is the first-order internal-multiple generator in the

Downloaded 04/08/16 to 129.215.249.201. Redistribution subject to SEG license or copyright; see Terms of Use at http://library.seg.org/

forward-scattering series. For a fixed source at $\mathbf{x}_s$ and a fixed receiver at $\mathbf{x}_r$, ten Kroode (2002) shows that $\mathbf{G}_0\mathbf{V}\mathbf{G}_0\mathbf{V}\mathbf{G}_0\mathbf{V}\mathbf{G}_0$ can be written in the following integral form:

$$d_3^{\mathrm{IM}}(\mathbf{x}_r,\mathbf{x}_s,\omega) \approx \int_{\substack{z_1>z_2\\ z_3>z_2}} G_0(\mathbf{x}_1,\mathbf{x}_s)V(\mathbf{x}_1)G_0(\mathbf{x}_2,\mathbf{x}_1)V(\mathbf{x}_2)G_0(\mathbf{x}_3,\mathbf{x}_2)V(\mathbf{x}_3) \times G_0(\mathbf{x}_r,\mathbf{x}_3)\mathrm{d}\mathbf{x}_1\mathrm{d}\mathbf{x}_2\mathrm{d}\mathbf{x}_3, \quad (6)$$

where d_3^{IM} denotes the set of all first-order internal multiples recorded at receiver $\mathbf{x}_r$ originating from a source at $\mathbf{x}_s$ (dependency on frequency ω has been omitted on the right side for conciseness). Unfortunately, in geophysical applications, equation 6 cannot usually be computed directly because it requires a priori information about the perturbation operator $\mathbf{V}$, also known as the reflectivity, at points throughout the volume spanned by the integral, which is not available (the reference Green's function G_0 may be computed because the reference model is generally known). Hence, we need to solve the inverse problem of equation 4 first to obtain $\mathbf{V}$ as a function of the data $\mathbf{D}$.

Inverse scattering and the internal-multiple generator

Equation 4 states that the data $\mathbf{D}$ can be expanded into an infinite series $\mathbf{D}=\sum_i\mathbf{D}_i$, where $\mathbf{D}_i$ is the portion of the data that is ith order in $\mathbf{V}$. Invoking the properties of the geometric series, Weglein et al. (1997) argue that in the inverse series, the reflectivity $\mathbf{V}$ can be expanded equivalently into $\mathbf{V}=\sum_i\mathbf{V}_i$, where $\mathbf{V}_i$ is the portion of $\mathbf{V}$ that is ith order in the data. By substituting $\mathbf{V}=\sum_i\mathbf{V}_i$ into equation 4, they find that

$$\mathbf{D}=\mathbf{G}_0(\mathbf{V}_1+\mathbf{V}_2+\dots)\mathbf{G}_0 + \mathbf{G}_0(\mathbf{V}_1+\mathbf{V}_2+\dots)\mathbf{G}_0(\mathbf{V}_1+\mathbf{V}_2+\dots)\mathbf{G}_0+\dots \quad (7)$$

$$=\mathbf{G}_0\mathbf{V}_1\mathbf{G}_0, \quad (8)$$

because all higher order terms cancel each other; for example,

$$\mathbf{G}_0\mathbf{V}_2\mathbf{G}_0+\mathbf{G}_0\mathbf{V}_1\mathbf{G}_0\mathbf{V}_1\mathbf{G}_0=0. \quad (9)$$

$$\mathbf{G}_0\mathbf{V}_3\mathbf{G}_0+\mathbf{G}_0\mathbf{V}_1\mathbf{G}_0\mathbf{V}_2\mathbf{G}_0+\mathbf{G}_0\mathbf{V}_2\mathbf{G}_0\mathbf{V}_1\mathbf{G}_0 + \mathbf{G}_0\mathbf{V}_1\mathbf{G}_0\mathbf{V}_1\mathbf{G}_0\mathbf{V}_1\mathbf{G}_0=0, \text{ etc.} \quad (10)$$

Equation 8 allows us to infer the subseries $\mathbf{V}_1$ directly from the data $\mathbf{D}$. In theory, all the other subseries could now be obtained sequentially: $\mathbf{V}_2$ from $\mathbf{V}_1$ using equation 9, $\mathbf{V}_3$ from $\mathbf{V}_1$ and $\mathbf{V}_2$ using equation 10, and so on. The sum of all subseries then provides the true reflectivity $\mathbf{V}$, which is the missing component in the internal-multiple generator (equation 6). Weglein et al. (1997), however, approximate $\mathbf{V}$ with its first subseries $\mathbf{V}_1$, which has the advantage that it can be directly computed from equation 8. The new multiples generator is thus $\mathbf{G}_0\mathbf{V}_1\mathbf{G}_0\mathbf{V}_1\mathbf{G}_0\mathbf{V}_1\mathbf{G}_0$.

A migration-demigration process

Following a more heuristic argument, ten Kroode (2002) states that $\mathbf{V}_1$ simply represents the common-shot migrated data, which is used as an approximation for the unknown reflectivity function $\mathbf{V}$ in equation 6. Assuming that $\mathbf{G}_0^{-1}\mathbf{G}_0=\mathbf{I}$, equation 8 becomes

$$\mathbf{V}_1=\mathbf{G}_0^{-1}\mathbf{D}\mathbf{G}_0^{-1}. \quad (11)$$

In reality, the above assumption might not be exactly true, but it is useful for the following thought experiment. Equation 11 is analogous to the so-called common-shot migration equation (equation 10 in ten Kroode, 2002). Using the Lippmann-Schwinger series as an alternative representation of $\mathbf{D}$ (equation 4), equation 11 can be written as

$$\mathbf{V}_1=\mathbf{G}_0^{-1}(\mathbf{G}_0\mathbf{V}\mathbf{G}_0+\mathbf{G}_0\mathbf{V}\mathbf{G}_0\mathbf{V}\mathbf{G}_0 + \mathbf{G}_0\mathbf{V}\mathbf{G}_0\mathbf{V}\mathbf{G}_0\mathbf{V}\mathbf{G}_0+\dots)\mathbf{G}_0^{-1}, \quad (12)$$

$$=\mathbf{V}+\mathbf{V}\mathbf{G}_0\mathbf{V}+\mathbf{V}\mathbf{G}_0\mathbf{V}\mathbf{G}_0\mathbf{V}+\dots, \quad (13)$$

which is consistent with ten Kroode's (2002) interpretation that $\mathbf{V}_1$ contains the true reflectivity ($\mathbf{V}$) plus erroneously imaged multiples ($\mathbf{V}\mathbf{G}_0\mathbf{V}+\mathbf{V}\mathbf{G}_0\mathbf{V}\mathbf{G}_0\mathbf{V}+\dots$).

In summary, the migration process (equation 11) provides an estimate of the reflectivity $\mathbf{V}_1$, given the data $\mathbf{D}$. The migrated data (i.e., the reflectivity estimate) $\mathbf{V}_1$ can then be used in the internal-multiple generator (equation 6) to replace the true reflectivity $\mathbf{V}$. The internal-multiple generator itself can be regarded as a demigration process that generates (part of) the data, given the reflectivity; Verschuur (2013) thus refers to Weglein's multiple estimation technique as a "migration-demigration process." This also makes it clear that the parameters used in the migration (e.g., the velocity of the reference medium) do not play an important role because errors

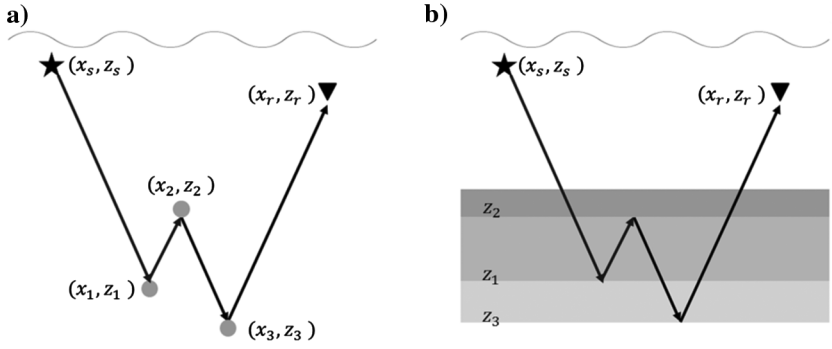

Figure 1. Example geometry for a third-order scattering event satisfying the LHL condition in a medium with (a) individual point scatterers and (b) horizontal reflectors. The star indicates the source location, and the inverted triangle indicates the receiver location; the background medium is water. The event in panel (b) represents an internal multiple of the kind we aim to predict.

Downloaded 04/08/16 to 129.215.249.201. Redistribution subject to SEG license or copyright; see Terms of Use at http://library.seg.org/

committed in migration will be balanced by the inverse process (demigration). The internal multiples can therefore be estimated from the recorded data alone.

Note that although it seems that the term chosen as the internal-multiple generator, $\mathbf{G}_0\mathbf{V}_1\mathbf{G}_0\mathbf{V}_1\mathbf{G}_0\mathbf{V}_1\mathbf{G}_0$, cancels out with other terms (equation 10) and thus does not contribute to the internal multiples in the data $\mathbf{D}$ (equation 7), we show in the "Discussion" section that, in fact, equation 7 contains multiple copies of scattered terms and that it is impossible to say which of those are canceled and which are preserved.

The internal-multiple equation

The final internal-multiple equation emerges from equation 6 after just one further modification: The second and third Green's functions on the right side of equation 6 are rewritten such that each of them could have been emitted or recorded at the measurement surface:

$$G_0(\mathbf{x}_2,\mathbf{x}_1) \approx \int G_0(\mathbf{x}_{r'},\mathbf{x}_1)G_0^*(\mathbf{x}_{r'},\mathbf{x}_2)\mathrm{d}\mathbf{x}_{r'}$$

$$\text{and} \quad G_0(\mathbf{x}_3,\mathbf{x}_2) \approx \int G_0(\mathbf{x}_3,\mathbf{x}_{s'})G_0^*(\mathbf{x}_2,\mathbf{x}_{s'})\mathrm{d}\mathbf{x}_{s'}, \tag{14}$$

where $\mathbf{x}_{r'}$ is an additional receiver location at the surface, $\mathbf{x}_{s'}$ is an additional source location, and * indicates complex conjugation. The term in the integrand of equation 14 is a crosscorrelation, which subtracts traveltimes in the phase term. It assumes that the background medium, in which G_0 is propagating, is smooth and that Green's functions' derivatives can be approximated by $n_i\partial_i G = \mp i\omega G$, with $-$ indicating outgoing waves and + indicating incoming waves at the boundary. Furthermore, integration boundaries are only partially available and it is assumed that a spatial tapering function has been applied to suppress contributions from the end points of the boundaries. Because the additional locations $\mathbf{x}_{r'}$ and $\mathbf{x}_{s'}$ are not known in advance, integration over a source boundary and a receiver boundary at the surface ($z = 0$) is required that provides contributions at the correct traveltimes following stationary phase arguments (ten Kroode, 2002). Using equation 14 and substituting V for V_1, equation 6 can be rearranged as

$$\begin{aligned} d_3^{\mathrm{IM}}(\mathbf{x}_r,\mathbf{x}_s) \approx \int_{\substack{z_1>z_2\\ z_3>z_2}} & [G_0(\mathbf{x}_1,\mathbf{x}_s)V_1(\mathbf{x}_1)G_0(\mathbf{x}_{r'},\mathbf{x}_1)] \\ & \times [G_0(\mathbf{x}_2,\mathbf{x}_{s'})V_1(\mathbf{x}_2)G_0(\mathbf{x}_{r'},\mathbf{x}_2)]^* \\ & \times [G_0(\mathbf{x}_3,\mathbf{x}_{s'})V_1(\mathbf{x}_3)G_0(\mathbf{x}_r,\mathbf{x}_3)]\mathrm{d}\mathbf{x}_1\mathrm{d}\mathbf{x}_2\mathrm{d}\mathbf{x}_3\mathrm{d}\mathbf{x}_{r'}\mathrm{d}\mathbf{x}_{s'}. \end{aligned} \tag{15}$$

Each term in brackets now stands for a primary wave reflected at $\mathbf{x}_1$, $\mathbf{x}_2$, and $\mathbf{x}_3$, respectively. Finally, ten Kroode (2002) expresses equation 15 in terms of the data D recorded at times t for the 1.5D case (2D wave propagation in a medium that varies only in one dimension) as

$$\begin{aligned} d_3^{\mathrm{IM}}(\mathbf{x}_r,\mathbf{x}_s,\omega) = (-i\omega)^2 & \int_{\substack{t_1>t_2\\ t_3>t_2}} D(\mathbf{x}_s,\mathbf{x}_{r'},t_1) \\ & \times D(\mathbf{x}_{s'},\mathbf{x}_{r'},t_2)D(\mathbf{x}_{s'},\mathbf{x}_r,t_3) \\ & \times \mathcal{A}(\mathbf{x}_s,\mathbf{x}_{s'},\mathbf{x}_r,\mathbf{x}_{r'},t_1,t_2,t_3)e^{i\omega(t_1-t_2+t_3)}\mathrm{d}t_1\mathrm{d}t_2\mathrm{d}t_3\mathrm{d}\mathbf{x}_{r'}\mathrm{d}\mathbf{x}_{s'}. \end{aligned} \tag{16}$$

For details about the amplitude factor $\mathcal{A}(\mathbf{x}_s,\mathbf{x}_{s'},\mathbf{x}_r,\mathbf{x}_{r'},t_1,t_2,t_3)$, the reader is referred to ten Kroode (2002). However, even without any knowledge of $\mathcal{A}$, correct kinematic information about first-order internal multiples can be inferred from equation 16. Note that in a 1D medium with a constant background velocity c_0 and a collocated source and receiver ($\mathbf{x}_r = \mathbf{x}_s$), $\mathcal{A}$ reduces to $(2/c_0)^2$. For this case, the stationary points $\mathbf{x}_{s'}$ and $\mathbf{x}_{r'}$ coincide with the source-receiver pair ($\mathbf{x}_s = \mathbf{x}_r = \mathbf{x}_{s'} = \mathbf{x}_{r'}$) and integration over source and receiver boundaries can be omitted. Thus, equation 16 becomes

$$d_3^{\mathrm{IM}}(\omega) = \left(\frac{-2i\omega}{c_0(0)}\right)^2 \int_{\substack{t_1>t_2\\ t_3>t_2}} D(t_1)D(t_2)D(t_3)e^{i\omega(t_1-t_2+t_3)}\mathrm{d}t_1\mathrm{d}t_2\mathrm{d}t_3. \tag{17}$$

In equations 16 and 17, the LHL condition (equation 5) has been transferred from depth to time, which is valid under the assumption of traveltime monotonicity,

$$z_1 > z_2 \Leftrightarrow \tau(\mathbf{x}_s;\alpha,z_1) > \tau(\mathbf{x}_s;\alpha,z_2), \tag{18}$$

where $\tau(\mathbf{x}_s;\alpha,z_i)$ is the traveltime of a ray starting at $\mathbf{x}_s$ under angle α, reflecting at depths z_i and traveling back to the surface. This condition tends to hold in media without strong lateral velocity variations, down to the maximum depth at which a ray with take-off angle α reflects.

Although equation 16 is derived from the first-order internal-multiple scattering term, the transformation of the LHL condition from depth to time makes it clear why also higher order multiples are automatically generated by this equation: Because the data D contains primaries and multiples, an event arriving at traveltime $t_3 > t_2$ could either be a primary that has a longer traveltime due to a deeper reflection point or an internal multiple that has a longer traveltime due to a longer (multiply reflected) propagation path. In the latter case, the combination of two primaries ($D(t_1)$ and $D(t_2)$) and a first-order multiple ($D(t_3)$) according to equation 16 results in an estimate of a second-order internal multiple. It should be noticed that there can be unfavorable combinations of primaries and internal multiples that, although consistent with the LHL criterion, may result in artifacts in the internal-multiple estimate, as discussed in Liang et al. (2013) and Ma and Weglein (2014).

Equation 16 is also valid in 2D cases under the assumptions of traveltime monotonicity and conormal reflectivity (ten Kroode, 2002), which means that the reflectivity $\mathbf{V}(\mathbf{x})$ is singular in the direction $n(\mathbf{x})$ only, where $\mathbf{x} \to n(\mathbf{x})$ is a smooth map from $\mathbf{R}^2$ to the unit circle. This is generally the case if the subsurface has a predominantly layered structure without point scatterers or angular boundaries.

Ten Kroode (2002) shows that the internal-multiple generator provided in equation 17 is equivalent to the 1D formula provided by Weglein et al. (1997, 2003)

$$b_3(k) = \int_{-\infty}^{\infty} \mathrm{d}z_1 e^{ikz_1}b(z_1) \int_{-\infty}^{z_1} \mathrm{d}z_2 e^{ikz_2}b(z_2) \int_{z_2}^{\infty} \mathrm{d}z_3 e^{ikz_3}b(z_3), \tag{19}$$

Downloaded 04/08/16 to 129.215.249.201. Redistribution subject to SEG license or copyright; see Terms of Use at http://library.seg.org/

where k denotes the vertical wavenumber and $b(z_i)$ is data with primaries and internal multiples in the so-called pseudodepth domain, i.e., after migration with the reference velocity of water.

In the following, ten Kroode's (2002) time-domain representation (equation 17) will be the basis for the comparison with the internal-multiple generator derived from SRI.

An equation for internal multiples derived from SRI

We will now derive the internal-multiple generator from SRI starting with a brief revision of the key equation and the main assumptions in SRI.

Introduction to SRI

The standard SRI equation in the monopole approximation gives an estimate of the homogeneous Green's function between a source at $\mathbf{x}_s$ and a receiver at $\mathbf{x}_r$ according to (Curtis and Halliday, 2010)

$$G(\mathbf{x}_r,\mathbf{x}_s,\omega)+G^*(\mathbf{x}_r,\mathbf{x}_s,\omega) \approx\frac{4}{(c\rho)^2}\int_S\int_{S'} G(\mathbf{x}_{r'},\mathbf{x}_s,\omega)G^*(\mathbf{x}_{r'},\mathbf{x}_{s'},\omega)G(\mathbf{x}_r,\mathbf{x}_{s'},\omega)\mathrm{d}\mathbf{x}_{r'}\mathrm{d}\mathbf{x}_{s'}. \tag{20}$$

The double integral is over two closed surface boundaries, S over sources $\mathbf{x}_{s'}$ and S' over receivers $\mathbf{x}_{r'}$, respectively. The integrand comprises the product of three Green's functions representing the wavefields propagating between the central source ($\mathbf{x}_s$) and the boundary receivers ($\mathbf{x}_{r'}$), between the boundary sources ($\mathbf{x}_{s'}$) and the boundary receivers ($\mathbf{x}_{r'}$), and between the boundary sources ($\mathbf{x}_{s'}$) and the central receiver ($\mathbf{x}_r$), respectively (Figure 2a). The * symbol denotes complex conjugation. Equation 20 is an approximation to an exact equation given in Curtis and Halliday (2010) because it is derived assuming that Green's functions' derivatives can be approximated by $n_i\partial_i G = \mp i\omega G$, as explained above. This holds if the boundaries S and S' are located in the far field of each other and of the central source-receiver pair, such that all raypaths can be assumed to be perpendicular to the boundaries.

Though in theory the boundaries are required to completely surround the central source-receiver pair ($\mathbf{x}_s$, $\mathbf{x}_r$), Snieder (2004) shows for interreceiver interferometry that the main contributions to the integral come from the parts of the boundary in which the integrand has approximately stationary phase, and contributions from elsewhere on the boundary cancel each other destructively. The same argument holds for SRI, which can be regarded as a concatenation of interreceiver interferometry and intersource interferometry (Curtis and Halliday, 2010; Curtis et al., 2012). Moreover, it has been shown (Löer et al., 2014) that linear surface boundaries (Figure 2b), as typically used in seismic exploration, span the stationary points needed to construct pseudophysical scattered wave energy from SRI, assuming that the scattering part of the medium is located below the source-receiver pair. The term pseudophysical denotes the fact that although traveltimes of the physical scattered wave energy are obtained correctly, amplitude and phase information of the constructed wavefield can be incorrect. If full boundaries are used and all theoretical requirements are fulfilled, pseudophysical and nonphysical contributions are combined in such a way to provide the physical wavefield as the final result of SRI. Thus, to obtain the physical scattered wavefield, stationary points that lie in the subsurface would have to be spanned by boundary sources and receivers, which is not practical in most experiments. It is therefore convenient to use pseudophysical energy as an estimate of the physical scattered wavefield.

By separating the direct arrival G_0 from the scattered field G_S using $G = G_0 + G_S$ (equation 1 assuming that the reference field contains no scattering heterogeneities), the SRI equation can be written as the sum of eight terms, in each of which different combinations of perturbed (scattered) and unperturbed fields are crosscorrelated and convolved. Löer et al. (2014) show for a single scatterer that the causal pseudophysical scattered wavefield can be constructed using only one of the eight terms, namely, the term that involves only scattered fields G_S. This also applies for media containing multiple scatterers or reflecting interfaces, the only drawback being that additional nonphysical energy is introduced in these cases. The latter notwithstanding, SRI therefore constructs the pseudophysical scattered wavefield between $\mathbf{x}_s$ and $\mathbf{x}_r$ from only the scattered components of the recorded wavefield and using only partial surface boundaries, and equation 20 becomes

$$\Phi(\mathbf{x}_r,\mathbf{x}_s,\omega) = \frac{4}{(c\rho)^2}\int_{S_{\mathrm{top}}}\int_{S'_{\mathrm{top}}} G_S(\mathbf{x}_{r'},\mathbf{x}_s,\omega) \times G_S^*(\mathbf{x}_{r'},\mathbf{x}_{s'},\omega)G_S(\mathbf{x}_r,\mathbf{x}_{s'},\omega)\mathrm{d}\mathbf{x}_{r'}\mathrm{d}\mathbf{x}_{s'}, \tag{21}$$

where S_{top} and S'_{top} denote the partial surface boundaries of sources and receivers as shown in Figure 2b. The scattered wavefields G_S on the right side correspond to the data D recorded at the measurement surface comprising primaries and internal multiples (the direct wave arrival and all surface-related multiples are assumed to have been removed). On the left side, $\Phi(\mathbf{x}_r,\mathbf{x}_s,\omega)$ denotes the constructed wavefield consisting of pseudophysical primaries and internal multiples and some nonphysical energy.

The multiple condition

To estimate internal multiples only (thus not primaries or nonphysical events), parts of the scattered Green's functions G_S are

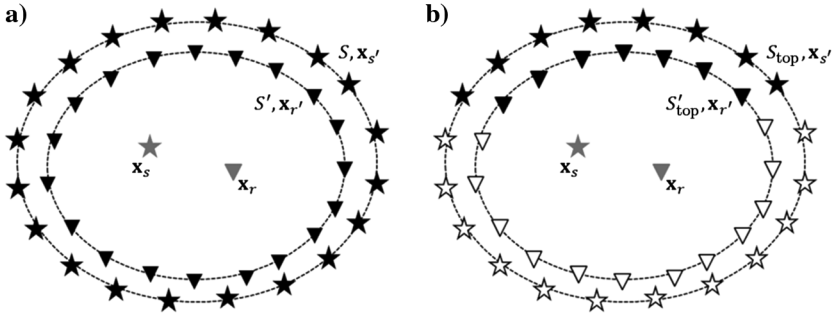

Figure 2. Conceptual geometry for SRI with (a) complete boundaries and (b) partial surface boundaries. Stars are sources, triangles are receivers; $\mathbf{x}_s$ and $\mathbf{x}_r$ denote the central source-receiver pair.

Downloaded 04/08/16 to 129.215.249.201. Redistribution subject to SEG license or copyright; see Terms of Use at http://library.seg.org/

used that satisfy a "multiple condition." If three primary events have been recorded as depicted in Figure 3 with traveltimes

$$t_1 > t_2 \quad \text{and} \quad t_3 > t_2\,, \tag{22}$$

Keydar et al. (1997) show that their traveltimes can be added and subtracted according to

$$t_M = t_1 - t_2 + t_3 \tag{23}$$

to yield the traveltime of an internal multiple t_M. The primaries are reflected at different depths, and each primary is associated with a different source-receiver pair. Note that the first primary and the second primary (with traveltimes t_1 and t_2, respectively) arrive at the same receiver location $\mathbf{x}_{r'}$) and that the second primary and the third primary (with traveltimes t_2 and t_3, respectively) start at the same source location $\mathbf{x}_{s'}$). These locations must be chosen such that parts of the raypaths of the first and the second primary, as well as of the second and the third primary, run parallel so that the corresponding traveltimes exactly cancel each other (see the dashed and solid lines in Figure 3a). In SRI, these locations correspond to the stationary points of the surface integrals, some of which are included automatically if we integrate over S_{top} and S'_{top}. This is also true if the source-receiver pair $[\mathbf{x}_s, \mathbf{x}_r]$ is included in the boundary, rather than being separated from or surrounded by it (compare Figures 2 and 3). Notice that if traveltime monotonicity (equation 18) holds, equation 22 is equivalent to the LHL condition in equation 5.

The internal-multiple equation

The following example shows how the multiple condition in equation 22 can be implemented inside the SRI equation to construct internal multiples only. Furthermore, it helps to establish a clear link between SRI and the internal-multiple equation derived from the ISS.

Let us consider the 1.5D case (2D wave propagation in a medium that varies only in one dimension) and a collocated source and receiver ($\mathbf{x}_s = \mathbf{x}_r$). For this case, the stationary points $\mathbf{x}_{s'}$ and $\mathbf{x}_{r'}$ coincide with the source-receiver pair ($\mathbf{x}_s = \mathbf{x}_r = \mathbf{x}_{s'} = \mathbf{x}_{r'}$) and integration over source and receiver boundaries can be omitted (in the infinite frequency approximation when the Fresnel zone is infinitesimal). Thus, equation 21 reduces to

$$\Phi(\omega) = \frac{4}{(c\rho)^2} D(\omega) D^*(\omega) D(\omega). \tag{24}$$

Here, the scattered wavefield G_S has been replaced by the data D, which equals G_S at the measurement surface. Equation 24 reproduces all primaries and multiples at frequency ω between a collocated source and receiver, plus some nonphysical artifacts. Next, we express equation 24 as the Fourier transform of the time-domain Green's functions:

$$\Phi(\omega) = \frac{4}{(c\rho)^2} \int_{-\infty}^{\infty} \mathrm{d}t_1 e^{i\omega t_1} D(t_1) \times \int_{-\infty}^{\infty} \mathrm{d}t_2 e^{-i\omega t_2} D(t_2) \int_{-\infty}^{\infty} \mathrm{d}t_3 e^{i\omega t_3} D(t_3). \tag{25}$$

This time-domain representation allows us to implement the multiple condition by modifying the integration boundaries of the second and third integral such that $t_1 > t_2$ and $t_3 > t_2$:

$$\Phi_{\text{IM}}(\omega) = \frac{4}{(c\rho)^2} \int_{-\infty}^{\infty} \mathrm{d}t_1 e^{i\omega t_1} D(t_1) \times \int_{-\infty}^{t_1-\epsilon_1} \mathrm{d}t_2 e^{-i\omega t_2} D(t_2) \int_{t_2+\epsilon_2}^{\infty} \mathrm{d}t_3 e^{i\omega t_3} D(t_3), \tag{26}$$

where $\Phi_{\text{IM}}(\omega)$ denotes the internal multiples at frequency ω and ϵ_1 and ϵ_2 are small positive numbers that account for the temporal width of the source signature of events. Equation 26 is the internal-multiple generator for the 1.5D case with a collocated source and receiver as derived from the SRI equation. As for the internal-multiple generator derived from the ISS, equation 26 can also predict higher order multiples due to the presence of multiples in the data D and the ambiguity inherent in the LHL condition in the time domain.

It is easy to show that equation 26 is equivalent to equation 17 given by ten Kroode (2002), which can be rearranged to

$$d_3^{\text{IM}}(\omega) = \left(\frac{-2i\omega}{c_0(0)}\right)^2 \int_{-\infty}^{\infty} \mathrm{d}t_1 e^{i\omega t_1} D(t_1) \int_{-\infty}^{t_1-\epsilon_1} \mathrm{d}t_2 e^{-i\omega t_2} D(t_2) \int_{t_2+\epsilon_2}^{\infty} \mathrm{d}t_3 e^{i\omega t_3} D(t_3). \tag{27}$$

The different prefactors in ours and ten Kroode's (2002) formula ($4/(c\rho)^2$ and $(-2i\omega/c_0(0))^2$, respectively) are due to different source types (volume injection rate in ours versus volume injection in ten Kroode's (2002) derivation — for details, see Wapenaar and Fokkema, 2006) and the fact that ten Kroode (2002) assumes a medium with constant density from

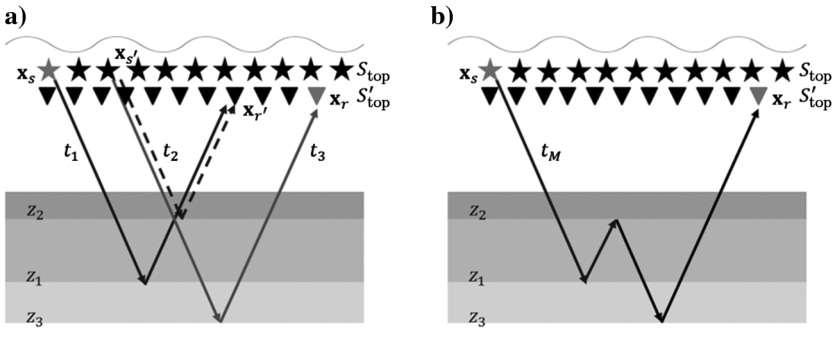

Figure 3. (a) Raypaths of primaries used in the multiple condition (equations 22 and 23). Portions of dashed and solid raypaths that run parallel cancel each other in SRI. (b) Raypath of the internal multiple with traveltime t_M that can be calculated from the traveltimes of the primaries in panel (a). Symbol key as in Figure 2.

Downloaded 04/08/16 to 129.215.249.201. Redistribution subject to SEG license or copyright; see Terms of Use at http://library.seg.org/

the beginning and therefore does not include ρ in his wave equation (equation 1 in ten Kroode, 2002).

Due to the pseudophysical nature of the single SRI term considered in equation 21, equation 26 provides the correct traveltimes of internal-multiple energy but amplitude and phase information of each multiple can be erroneous. Similarly, Weglein et al. (2003) argue that amplitudes of internal multiples estimated from the ISS are wrong because only a subseries of the ISS is considered that estimates internal multiples to first order only. Thus, in neither method is the final equation used the one that represents how multiples are actually constructed by SRI or the ISS, explaining from two quite different points of view why equations 26 and 27 do not produce exactly correct physical results. Nevertheless, we show next that the insights gained from linking the ISS to SRI allow a significantly different and computationally far more efficient representation for multiple prediction in the ISS and the SRI frameworks.

An alternative representation

The SRI equation (equation 21 or 24) is a combination of correlation-type interreceiver interferometry and convolution-type intersource interferometry. Crosscorrelation and convolution in the frequency domain are vector multiplications that are fast and cheap to compute. It would therefore be favorable if we could rewrite the internal-multiple equation (equation 26), which is based on the SRI equation, in a way that allows us to carry out these two operations separately, one after the other, in the frequency domain to reduce computational cost. In this chapter, a new representation is derived that achieves this by using an alternative implementation of the multiple condition.

Correlation- and convolution-type representation of internal multiples

We start by identifying the correlational and convolutional operations in the 1D SRI equation (equation 24) and the derived internal-multiple equation (equation 26). In the frequency domain, a crosscorrelation $C(\omega)$ corresponds to a simple multiplication of two functions $f(\omega)$ and $g(\omega)$, where one of the two functions has been complex conjugated. In the time domain, crosscorrelation of two functions $f(t)$ and $g(t)$ is given by

$$C(\tau) = \int_{-\infty}^{\infty} f(t)g(t+\tau)\mathrm{d}t, \tag{28}$$

where τ is a time shift parameter. In equation 24, the correlational part is given by the multiplication of the term $D^*(\omega)$ with either of the other two terms $D(\omega)$; without loss of generality, we will take the rightmost term. The corresponding time-domain integrals in equation 26 can be rewritten by analogy with equation 28 by introducing a time shift parameter τ and substituting the integration variable t_3 for $t_2+\tau$. Interchanging the order of integration, the rightmost two integrals can be written as

$$\int_{-\infty}^{t_1-\epsilon_1} \mathrm{d}t_2 e^{-i\omega t_2} D(t_2) \int_{t_2+\epsilon_2}^{\infty} \mathrm{d}t_3 e^{i\omega t_3} D(t_3) = \int_{\epsilon_2}^{\infty} e^{i\omega\tau} \int_{-\infty}^{t_1-\epsilon_1} D(t_2)D(t_2+\tau)\mathrm{d}t_2\ \mathrm{d}\tau. \tag{29}$$

The inner integral on the right side of equation 29 resembles a crosscorrelation at time shift τ. However, the upper integration boundary is set to $t_1-\epsilon_1$ rather than to ∞. This is an important point that will be addressed later. Similarly, the outer integral over τ resembles a Fourier transform but again one integration boundary, here the lower one, is incorrect.

The purpose of the restricted lower boundary is to ensure that when the correlation results for different time shifts τ are summed, only positive time shifts $\tau \geq \epsilon_2$ are considered. With $t_3 = t_2+\tau$, this condition is equivalent to the part of the multiple condition stating that $t_3 > t_2$. An alternative way to implement this condition is to invoke the Heaviside step function $H(\tau-\epsilon_2)$ that takes a value of one for positive arguments and zero for negative arguments (note that we follow the convention $H(0)=1$). Hence, the restriction of the lower integration boundary becomes obsolete and the crosscorrelation part can be written as

$$\int_{-\infty}^{\infty} e^{i\omega\tau}\Gamma_{\text{causal}}(\tau;t_1)\mathrm{d}\tau = \int_{-\infty}^{\infty} e^{i\omega\tau}\ H(\tau-\epsilon_2) \times \int_{-\infty}^{t_1-\epsilon_1} D(t_2)D(t_2+\tau)\mathrm{d}t_2\ \mathrm{d}\tau, \tag{30}$$

where the function $\Gamma_{\text{causal}}(\tau;t_1)$ represents the causal part of the correlation-type integral over t_2 that is zero for $\tau < \epsilon_2$. The left side of equation 30 is used to replace the latter two terms in the internal-multiple equation, equation 26, which yields

$$\Phi_{\text{IM}}(\omega) = \frac{4}{(c\rho)^2}\int_{-\infty}^{\infty} e^{i\omega t_1} D(t_1) \int_{-\infty}^{\infty} e^{i\omega\tau}\Gamma_{\text{causal}}(\tau;t_1)\mathrm{d}\tau\mathrm{d}t_1. \tag{31}$$

Thus, we have expressed part of the internal-multiple equation by the correlation-type function $\Gamma_{\text{causal}}(\tau;t_1)$. Next, we show that equation 31 is equivalent to a convolution-type function. Convolution in the time domain is defined as

$$C'(\tau') = \int_{-\infty}^{\infty} f(t)g(\tau'-t)\mathrm{d}t. \tag{32}$$

As before, we change the integration variable of the inner integral in equation 31 by introducing a new time shift parameter $\tau = \tau' - t_1$. Rearranging the terms yields

$$\Phi_{\text{IM}}(\omega) = \frac{4}{(c\rho)^2}\int_{-\infty}^{\infty} e^{i\omega\tau'} \int_{-\infty}^{\infty} D(t_1)\Gamma_{\text{causal}}(\tau'-t_1;t_1)\mathrm{d}t_1\mathrm{d}\tau'. \tag{33}$$

The inner integral is equivalent to a convolution in the time domain, whereas the outer integral is a standard Fourier transformation from the time to the frequency domain.

Crosscorrelation and convolution uncoupled

Thus far, we have shown explicitly how the formula that estimates internal multiples (equation 26) can be written as a concatenation of a

Downloaded 04/08/16 to 129.215.249.201. Redistribution subject to SEG license or copyright; see Terms of Use at http://library.seg.org/

correlation-type function (equation 30) and a convolution-type function (equation 33). However, in the current form of equation 33, the two are coupled through the argument of the correlation-type function Γ_{causal}, which depends on the integration variable of the convolution-type function t_1. We now show how the two operations can be uncoupled and performed independently in the frequency domain to save computation time and cost.

First, we substitute the correlation-type function Γ_{causal} in equation 33 for the corresponding integral expression (right side of equation 30):

$$\Phi_{\text{IM}}(\omega) = \frac{4}{(c\rho)^2}\int_{-\infty}^{\infty} e^{i\omega\tau'}\int_{-\infty}^{\infty} D(t_1) \times H(\tau' - t_1 - \epsilon_2)\int_{-\infty}^{t_1-\epsilon_1} D(t_2)D(t_2 + (\tau' - t_1))\mathrm{d}t_2\mathrm{d}t_1\mathrm{d}\tau'. \tag{34}$$

The coupling of convolution and crosscorrelation is implicit in the upper boundary of the innermost integral, which depends on the integration variable of the surrounding integral (t_1). With a few modifications, however, this can be changed: Due to the Heaviside function $H(\tau' - t_1 - \epsilon_2)$, the integral over t_1 is zero if $\tau' - t_1 - \epsilon_2 < 0$, hence for all $t_1 > \tau' - \epsilon_2$. We can thus truncate the first data vector $D(t_1)$ and keep only the part of D for which $t_1 \le \tau' - \epsilon_2$ (reducing the length of the data also saves computation time). Substituting $t_1 \le \tau' - \epsilon_2$ into $t_2 \le t_1 - \epsilon_1$ (the upper boundary of the innermost integral) yields $t_2 \le \tau' - \epsilon_2 - \epsilon_1$ and consequently $t_2 \le \tau' - \epsilon_2$ (because ϵ_1 and ϵ_2 are positive); hence, we can also truncate the second data vector $D(t_2)$ and keep only the part for which $t_2 \le \tau' - \epsilon_2$. The argument of the third D is $t_3 = t_2 + \tau' - t_1$. From $t_2 \le t_1 - \epsilon_2$, it follows that $t_3 \le \tau' - \epsilon_2$ and again we keep only the part of D for times $t_3 \le \tau' - \epsilon_2$. This gives

$$\Phi_{\text{IM}}(\omega) = \frac{4}{(c\rho)^2}\int_{-\infty}^{\infty} e^{i\omega\tau'}\int_{-\infty}^{\infty} D_{m(\tau')}(t_1)H(\tau' - t_1 - \epsilon_2) \times \int_{-\infty}^{t_1-\epsilon_1} D_{m(\tau')}(t_2)D_{m(\tau')}(t_2 + (\tau' - t_1))\mathrm{d}t_2\mathrm{d}t_1\mathrm{d}\tau', \tag{35}$$

where notation $D_{m(\tau')}(t_i)$ means that data in D have been muted for times $t_i > \tau' - \epsilon_2$. The Heaviside function $H(\tau' - t_1 - \epsilon_2)$ can now be dropped because $\tau' - t_1 - \epsilon_2 \ge 0$ is equivalent to $t_1 \le \tau' - \epsilon_2$, which is implicit by muting the data. The restricted integration boundary is obsolete, too; however, this step might not be obvious at first sight: although the second data vector D is truncated and therefore $t_2 \le \tau' - \epsilon_2$, replacing $t_1 - \epsilon_1$ by ∞ in the upper integration boundary allows $t_1 - \epsilon_1 < t_2 \le \tau' - \epsilon_2$, which seems to contradict the multiple condition $t_2 < t_1$. However, considering the third data vector $D(t_2 + \tau' - t_1)$, we find that for $t_2 > t_1 - \epsilon_1$, the argument of D is larger than $\tau' - \epsilon_1$, which gives a zero contribution due to muting. In fact, this is also valid for $t_1 - \epsilon_1 < t_2 < \infty$, which means that truncating the second D is not necessary at all but is done for consistency and to reduce the length of the vector and thus the computation time. We can, therefore, write the alternative internal-multiple equation according to

$$\Phi_{\text{IM}}(\omega) = \frac{4}{(c\rho)^2}\int_{-\infty}^{\infty} e^{i\omega\tau'}\int_{-\infty}^{\infty} D_{m(\tau')}(t_1) \times \int_{-\infty}^{\infty} D_{m(\tau')}(t_2)D_{m(\tau')}(t_2 + (\tau' - t_1))\mathrm{d}t_2\mathrm{d}t_1\mathrm{d}\tau'. \tag{36}$$

For each τ', the correlational integral (over t_2) and the convolutional integral (over t_1) can now be evaluated separately, one after the other. This allows us to perform these operations in the frequency domain where they correspond to simple vector multiplications that are fast and cheap to compute.

The Fourier integral over τ' can be interpreted as an integral over possible multiple traveltimes t_M: only if $\tau' = t_M$ the multiple condition $t_M = t_1 - t_2 + t_3$ is fulfilled, and the contribution of the integral is nonzero. Note that the multiple condition (equation 23) can be found explicitly in the argument of the third D: $t_2 + (t_M - t_1) = t_3 \Leftrightarrow t_M = t_1 - t_2 + t_3$.

The additional constraints described in equation 22, $t_1 > t_2$ and $t_3 > t_2$, are also implicit by allowing only $t \le \tau' - \epsilon_2$ because

$$t_3 \le \tau' - \epsilon_2 \wedge t_3 = t_2 + (\tau' - t_1) \Rightarrow t_2 \le t_1 - \epsilon_2, \tag{37}$$

and

$$t_1 \le \tau' - \epsilon_2 \wedge t_3 = t_2 + (\tau' - t_1) \Rightarrow t_2 \le t_3 - \epsilon_2. \tag{38}$$

In summary, for a collocated source and receiver, the internal multiple arriving at time τ' can be computed by performing the following steps:

1) Cut the data $D(t)$ above $t = \tau' - \epsilon_1$ to obtain $D_{m(\tau')}(t)$.
2) Transform $D_{m(\tau')}(t)$ to the frequency domain to obtain $D_{m(\tau')}(\omega)$, then multiply $D_{m(\tau')}(\omega)$ with its complex conjugate $D^*_{m(\tau')}(\omega)$ (corresponds to an autocorrelation in the time domain), the result of which is $\Gamma(\omega)$.
3) Multiply $\Gamma(\omega)$ with $D_{m(\tau')}(\omega)$ (corresponds to a convolution in the time domain) and transform the result to the time domain to obtain $\Phi_{\text{IM}}(\tau')$.
4) Repeat steps 1–3 for all lag times τ' to obtain an estimate of all internal multiples.

This gives the result in the time domain; i.e., the outermost integration in equation 36 (the Fourier transform from time to frequency) is not performed. When considering a common-shot gather, we need to reassign the geometric parameters (source and receiver positions) to the data and integrate over source and receiver boundaries S and S', respectively, as shown by SRI in equations 20 and 21. This yields

$$\Phi_{\text{IM}}(\mathbf{x}_r, \mathbf{x}_s, \omega) = \frac{4}{(c\rho)^2}\int_S \mathrm{d}\mathbf{x}_{s'}\int_{S'} \mathrm{d}\mathbf{x}_{r'} \times \int_{-\infty}^{\infty} \mathrm{d}\tau' e^{i\omega\tau'}\int_{-\infty}^{\infty} \mathrm{d}t_1 D_{m(\tau')}(\mathbf{x}_{r'}, \mathbf{x}_s, t_1) \times \int_{-\infty}^{\infty} \mathrm{d}t_2 D_{m(\tau')}(\mathbf{x}_{r'}, \mathbf{x}_{s'}, t_2)D_{m(\tau')}(\mathbf{x}_r, \mathbf{x}_{s'}, t_2 + (\tau' - t_1)). \tag{39}$$

Downloaded 04/08/16 to 129.215.249.201. Redistribution subject to SEG license or copyright; see Terms of Use at http://library.seg.org/

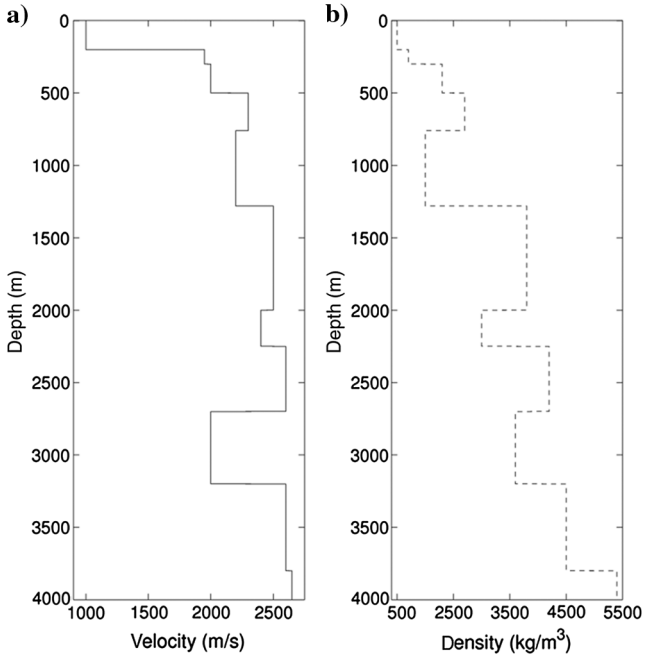

Figure 4. (a) Velocity profile and (b) density profile of the acoustic model used to generate synthetic data sets.

Note that in this case instead of performing an autocorrelation in step 2, we need to crosscorrelate the correct portions of the data, namely, $D_{m(\tau')}(\mathbf{x}_{r'}, \mathbf{x}_{s'}, t)$ and $D_{m(\tau')}(\mathbf{x}_r, \mathbf{x}_{s'}, t)$. In the 3D case, the integration boundaries over $\mathbf{x}_{s'}$ and $\mathbf{x}_{r'}$ span 2D surfaces rather than 1D lines.

NUMERICAL EXAMPLES

Using a set of MATLAB codes, we estimate internal multiples for the 1.5D case following (1) Weglein's formulation from the ISS version, (equations 16 and 17) and (2) the new representation from SRI (equations 36 and 39), both of which are mathematically equivalent. For a synthetic data set based on an acoustic 10-layer model (Figure 4) provided by Total S.A., we verify the qualitative equivalence of both methods and compare them in terms of computational cost.

Examples from a synthetic data set

Figures 5 and 6 show the results for a collocated source and receiver using the ISS (equation 17) and SRI (equation 36), respectively. Displayed in Figures 5a and 6a are the modeled scattered wavefield G_S (gray) in the time window between 0 and 2 s. Surface-related multiples have not been modeled. Superimposed is

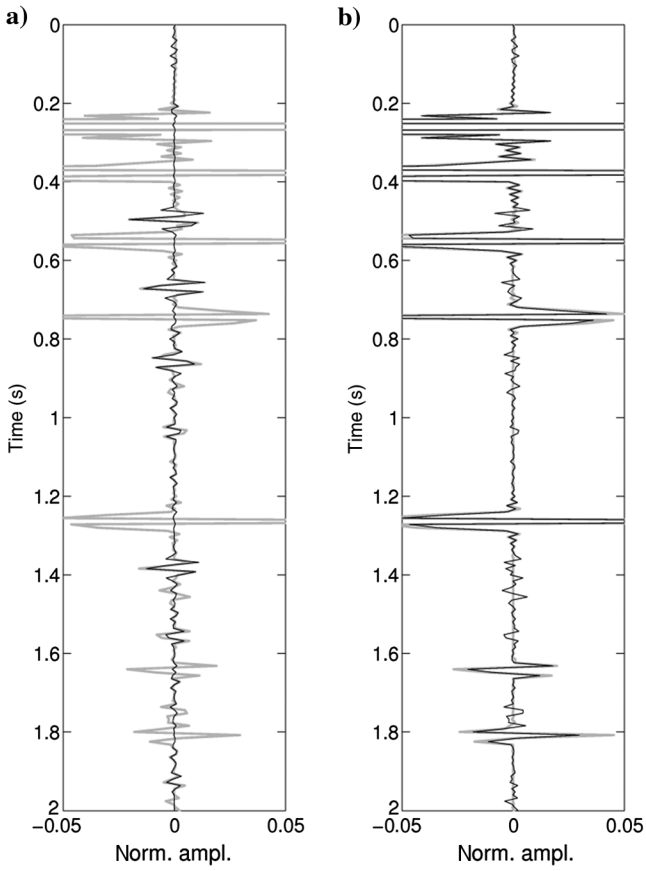

Figure 5. Internal multiples estimated from the ISS (equation 17) for a collocated source and receiver. (a) Estimate of internal multiples (black) compared to the full scattered wavefield (gray). (b) Demultipled scattered field (black) compared to the primary wavefield (gray).

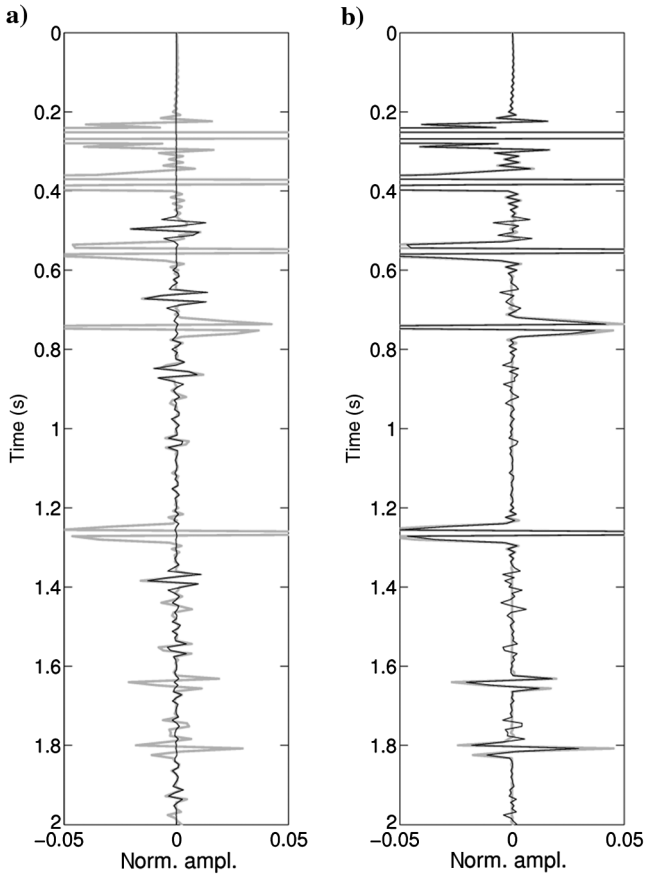

Figure 6. Internal multiples estimated from SRI (equation 36) for a collocated source and receiver. (a) Estimate of internal multiples (black) compared to the full scattered wavefield (gray). (b) Demultipled scattered field (black) compared to the primary wavefield (gray).

Downloaded 04/08/16 to 129.215.249.201. Redistribution subject to SEG license or copyright; see Terms of Use at http://library.seg.org/

the internal-multiple estimate (black). The amplitude factors in both equations have been ignored; instead, the first-arriving multiple was normalized with respect to the amplitude of the original trace at the same arrival time. This underlines the similarity between true and estimated multiples regardless of errors in the absolute amplitude. In Figures 5b and 6b, the internal-multiple estimate has been subtracted from the scattered wavefield and the result (black) is compared with the directly modeled primary wavefield (gray). The small wiggles at the beginning of the computed traces in Figure 5 are likely to be numerical inaccuracies due to the Fourier transform from the frequency to the time domain using only a finite number of frequencies and are not related to the formula itself. In Figure 6, this effect is not observed due to the different structure of the SRI-based formula with the Fourier transform from frequency to time applied to each time step rather than to the final results.

Figure 7 shows internal-multiple estimates for a common-shot gather in the time window between 0 and 1s from a source at $z = 5$ and $x = 12.5$ m recorded at nine receivers located at the same depth between $x = 12.5$ and 212.5 m with interreceiver spacing of 25 m, where x is the horizontal coordinate axis. Boundary sources and receivers were distributed as linear arrays at depth $z = 5$ m between $x = 0$ and 237.5 m with spacing of 12.5m. The same velocity-density model has been used (Figure 4). Figure 7a and 7b shows the full scattered wavefield (gray) superimposed by the internal multiples estimated using the ISS (equation 16) and SRI (equation 39), respectively. Figure 7c compares the internal multiples from the two different equations directly. The few small differences at the beginning of each trace are likely to be due to the finite number of frequencies computed using the ISS, which affects the Fourier transformation to the time domain. Figure 8 shows the demultipled common-shot gathers compared to the directly modeled primary wavefield using the ISS equation (Figure 8a) and the SRI equation (Figure 8b).

Computational cost

We calculated the computational cost (number of operations) for both methods for the case of a single trace (1D medium, collocated source, and receiver) and compare the results in Figure 9: The solid line gives the number of operations required in the ISS formalism as a function of the number of time samples N (i.e., the length of the traces) according to

$$N * 3 * \left[\frac{1}{6}N(N-1)[2(N-1)+1]\right] + \left(\frac{N}{2}\log_2 N\right). \quad (40)$$

This formula can be explained as follows: The underlying equation for the computation of internal multiples in a 1D medium

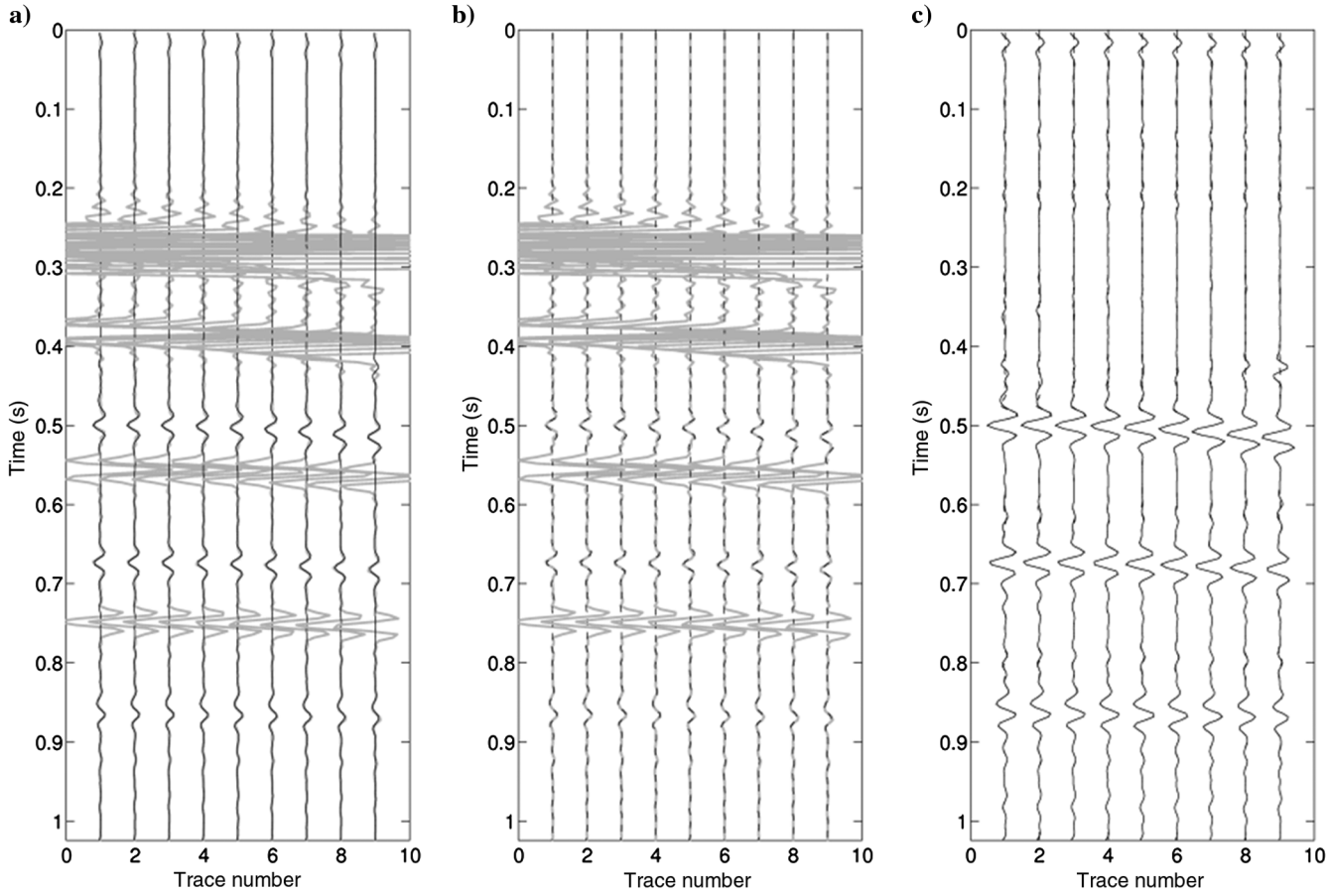

Figure 7. Estimate of internal multiples for a common-shot gather. Details on the geometry are described in the main text. (a) Full scattered wavefield (gray) versus internal multiples estimated from the ISS equation (black). (b) Full scattered wavefield (gray) versus internal multiples estimated from the SRI equation (dashed black). (c) Internal multiples from the ISS (solid) versus internal multiples from SRI (dashed).

Downloaded 04/08/16 to 129.215.249.201. Redistribution subject to SEG license or copyright; see Terms of Use at http://library.seg.org/

(equation 17) has to be computed for each frequency individually. Because the number of frequencies is equal to the number of time samples, this gives a factor N. Further, equation 17 consists of three nested integrals over traveltimes t_1, t_2, and t_3, respectively. Each time the innermost integrand is computed, three operations are carried out, namely, the multiplication of $D(t_1)$, $D(t_2)$, $D(t_3)$, and $\exp[i\omega(t_1 - t_2 + t_3)]$, hence the factor 3. The term in square brackets in equation 40 equals the sum of squares of natural numbers between 1 and $N-1$ ($\sum_{n=1}^{N-1} n^2$) and tells us how many times this integrand is computed. Were all three integrals to be computed over the full range of N time samples, this would simply contribute a factor N^3. However, we have to take into account that $t_1 > t_2$ and $t_3 > t_2$. For example, if $t_2 = n\Delta t$ (where Δt is the inverse of the sampling rate and $n \in [1, N-1]$), then t_1 and t_3 can only have values greater than $n\Delta t$ so that the integrand has to be computed $(N-n)^2$ times; for $t_2 = 1\Delta t$, it is computed $(N-1)^2$ times; and for $t_2 = (N-1)\Delta t$, it is computed only once ($[N-(N-1)]^2 = 1$). Hence, a total of $(N-1)^2 + (N-2)^2 + \ldots + 1^2 = \sum_{n=1}^{N-1} n^2 = 1/6(N-1)N[2(N-1)+1]$ operations is required. Finally, the term in round brackets accounts for the number of operations performed in the Fourier transform to the time domain. By slightly modifying the internal-multiple equation in the ISS formal-

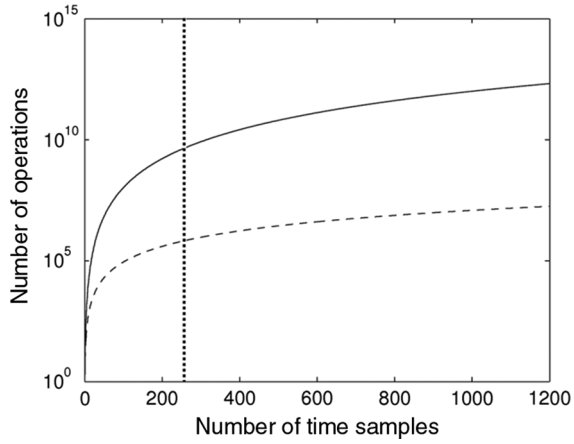

Figure 9. Computational cost as a function of the number of time samples using the ISS formula (equation 17; solid line) and the SRI formula (equation 36; dashed line) for internal-multiple prediction in a 1D medium with a collocated source-receiver pair. The vertical dotted line indicates the computational cost for a trace with length $N = 256$. More details are provided in the main text.

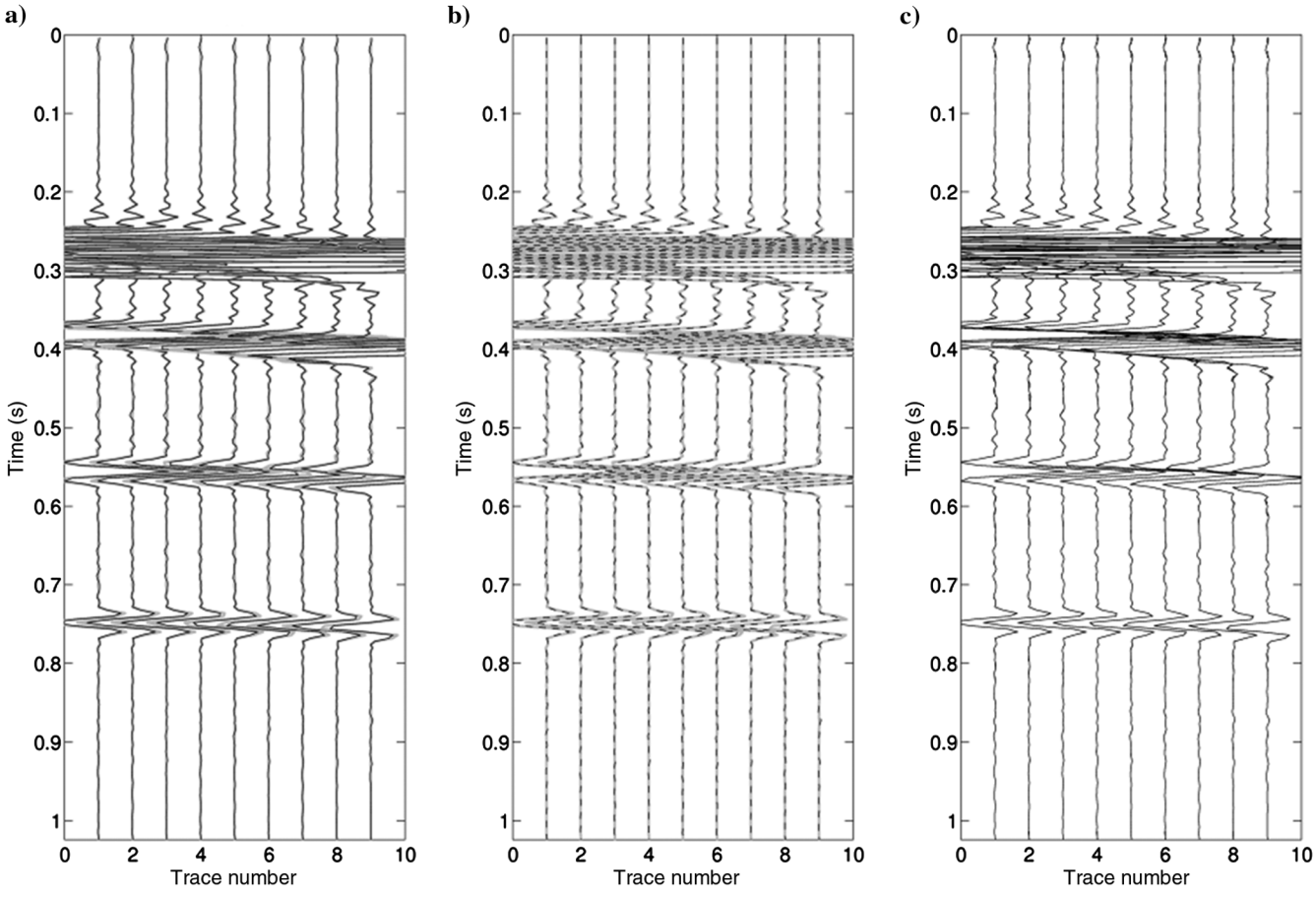

Figure 8. Demultipled scattered wavefield for a common-shot gather compared to the directly modeled primary wavefield (gray) using (a) the ISS equation (black solid) and (b) the SRI equation (black dashed). (c) Demultipled data from the ISS (solid) versus demultipled data from SRI (dashed).

Downloaded 04/08/16 to 129.215.249.201. Redistribution subject to SEG license or copyright; see Terms of Use at http://library.seg.org/

ism, Kaplan et al. (2005) show that the computational cost can be reduced by a factor N.

The dashed line in Figure 9 gives the number of operations required when using the alternative formula (equation 36, or following the four steps outlined above) as a function of the number of time samples N according to

$$N * \left[2\left(\frac{N}{2}\log_2 N\right) + 2N\right]. \quad (41)$$

The first factor N stands for the number of time lags τ' and is equal to the total number of time samples. The factor 2 denotes the number of Fourier transforms, and the term in round brackets denotes the number of operations carried out in one Fourier transform. The factor $2N$ accounts for the crosscorrelation and convolution in the frequency domain, which corresponds to elementwise multiplication of two vectors of length N.

For a single trace (the case of a collocated source and receiver) with 256 time samples (or 256 frequencies), the number of operations performed by the ISS equation is of the order of 10^9, whereas the SRI equation requires of the order of 10^5 operations (see the vertical dotted line in Figure 9). For the ISS version, this results in a computing time of approximately 245 s on a standard desktop computer without parallelization (approximately 75 s when parallelized over four workers), whereas the SRI version provides the same result in 0.25 s unparallelized. Figure 9 shows that the difference in the number of operations increases with the number of time samples used. This difference becomes even more important when the source and the receiver are not collocated; to compute the internal multiples between a source at $\mathbf{x}_s$ and a receiver at $\mathbf{x}_r \neq \mathbf{x}_s$, both methods require integration over a source boundary and a receiver boundary to cover the additional source-receiver pair $[\mathbf{x}_{s'}, \mathbf{x}_{r'}]$ that is involved in the corresponding equations. The computation time for a single source-receiver pair is multiplied by the product of the number of sources $N_{s'}$ and the number of receivers $N_{r'}$ on the boundaries. Hence, for $N_{s'} = 30$ boundary sources and $N_{r'} = 30$ boundary receivers, the computation time is $N_{s'} \cdot N_{r'} = 900$ times as long in SRI and ISS as in the single-trace case. Moreover, to compute multiples in a common-shot gather rather than for a single trace, the computation time is multiplied by the number of traces N_r in the gather. Because both methods are multiplied by the same factor $N_{s'} \cdot N_{r'} \cdot N_r$, the relative computational cost remains $(\text{cost}_{\text{ISS}}/\text{cost}_{\text{SRI}}) \sim 10^9/10^5 = 10^4$, whereas the cost in absolute number of operations taken for a gather is $\sim 10^4 \times N_{s'} \times N_{r'} \times N_r$, which for the case above with $N_{s'} = N_{r'} = 30$ and for a gather of only $N_r = 20$ traces results in a saving of $10^4 \times 30 \times 30 \times 20 \sim 10^8$ operations per gather using SRI compared to the ISS. In the 3D case, the factors $N_{s'}$, $N_{r'}$, and N_r would usually increase by an order of magnitude each, leading to another saving of 10^3 operations per gather.

DISCUSSION

Forward-scattering theory, as described by the Lippmann-Schwinger equation, provides an estimate of the data given the reflectivity of the medium. The equation can be expanded into an infinite series, and Weglein et al. (1997) take one term out of this series, namely the third-order scattering term, as the basis for internal-multiple prediction. However, the third-order scattering term provides only a first-order estimate to first-order internal scattering; higher order contributions come from the fifth, the seventh, etc. order terms. The fifth-order term is analyzed by Ramírez and Weglein (2005) who show that, indeed, amplitude estimates can be improved by taking such higher order terms into account.

Further, we mention that the term used to estimate internal multiples by Weglein et al. (1997) seems to cancel out destructively with other terms and apparently does not contribute to the internal multiples in the data. We now show that the term does indeed contain information about multiples and how this provides another link to interferometry.

Inserting the representation of $\mathbf{V}_1$ provided in equation 13 into the internal-multiple generator yields the following:

$$\begin{aligned}
&\mathbf{G}_0\mathbf{V}_1\mathbf{G}_0\mathbf{V}_1\mathbf{G}_0\mathbf{V}_1\mathbf{G}_0 \\
&\quad = \mathbf{G}_0(\mathbf{V} + \mathbf{V}\mathbf{G}_0\mathbf{V} + \ldots)\mathbf{G}_0(\mathbf{V} + \mathbf{V}\mathbf{G}_0\mathbf{V} + \ldots) \\
&\mathbf{G}_0(\mathbf{V} + \mathbf{V}\mathbf{G}_0\mathbf{V} + \ldots)\mathbf{G}_0 \\
&\quad = \mathbf{G}_0\mathbf{V}\mathbf{G}_0\mathbf{V}\mathbf{G}_0\mathbf{V}\mathbf{G}_0 + 3(\mathbf{G}_0\mathbf{V}\mathbf{G}_0\mathbf{V}\mathbf{G}_0\mathbf{V}\mathbf{G}_0\mathbf{V}\mathbf{G}_0) \\
&\quad + 6(\mathbf{G}_0\mathbf{V}\mathbf{G}_0\mathbf{V}\mathbf{G}_0\mathbf{V}\mathbf{G}_0\mathbf{V}\mathbf{G}_0\mathbf{V}\mathbf{G}_0) \\
&\quad + 7(\mathbf{G}_0\mathbf{V}\mathbf{G}_0\mathbf{V}\mathbf{G}_0\mathbf{V}\mathbf{G}_0\mathbf{V}\mathbf{G}_0\mathbf{V}\mathbf{G}_0\mathbf{V}\mathbf{G}_0) \\
&\quad + 9(\mathbf{G}_0\mathbf{V}\mathbf{G}_0\mathbf{V}\mathbf{G}_0\mathbf{V}\mathbf{G}_0\mathbf{V}\mathbf{G}_0\mathbf{V}\mathbf{G}_0\mathbf{V}\mathbf{G}_0\mathbf{V}\mathbf{G}_0) + \ldots. \quad (42)
\end{aligned}$$

The result corresponds to the true internal-multiple generator (the third-order scattering term of the Lippmann-Schwinger equation, $\mathbf{G}_0\mathbf{V}\mathbf{G}_0\mathbf{V}\mathbf{G}_0\mathbf{V}\mathbf{G}_0$), plus multiple versions of higher order scattering terms. As also pointed out by ten Kroode (2002), the errors caused by the additional higher order contributions are likely to be small compared to the internal multiples. We thus conclude that despite the fact that all information seems to be contained in $\mathbf{G}_0\mathbf{V}_1\mathbf{G}_0$, the third-order scattering term $\mathbf{G}_0\mathbf{V}_1\mathbf{G}_0\mathbf{V}_1\mathbf{G}_0\mathbf{V}_1\mathbf{G}_0$ also generates internal multiples and that after the summation of all terms (equation 7), some of them must cancel to provide the correct, physical result. It is, however, impossible to define which terms are canceled and which are preserved. This is why it is reasonable to use this term to estimate internal multiples.

In interferometry, so-called pseudophysical energy (Löer et al., 2014) can be used as an estimate for physically scattered waves. We mentioned above that the SRI equation can be written as the sum of eight terms, in which different combinations of perturbed and unperturbed (scattered) fields are crosscorrelated and convolved. Meles and Curtis (2013) and Löer et al. (2014) investigate the different contributions from each term to the final result for a single scatterer case. They show, for example, that there is one term that provides a physical scattered wave, but at the same time gives rise to a nonphysical contribution from a different stationary point pair on the source and receiver boundaries. The nonphysical part is canceled by the contributions from other terms, a phenomenon that has also been discussed for interreceiver interferometry, for example, by Snieder et al. (2008). Similarly, pseudophysical energy, which has the same kinematics as physical energy but the wrong amplitude (and in some cases also a wrong phase), is provided by several terms of the SRI equation, and only their sum provides the correct physical wavefield. Thus, although pseudophysical energy arrives at the same time as physical energy, an individual pseudo-

Downloaded 04/08/16 to 129.215.249.201. Redistribution subject to SEG license or copyright; see Terms of Use at http://library.seg.org/

physical term does not necessarily provide the correct (physical) amplitude and phase.

If not all of the terms are used, or not all stationary point pairs are spanned by the portions of boundaries included in SRI, the summation of pseudophysical energy may be incomplete and, hence, the physical result cannot be obtained. This is exactly what happens when SRI is used to estimate internal multiples herein: only one out of eight terms is considered, and boundaries are available only at the surface. Under these conditions, only one pseudophysical term contributes, which emulates the kinematics of a physical scattered wavefield but does not provide the correct amplitude information.

Thus, in the SRI and ISS approaches, internal multiples are estimated from pseudophysical energy and hence cannot be used to estimate and eliminate the internal multiples in the data directly. An adaptive subtraction algorithm is required to find the best fit between estimated and true multiples and eventually attenuate the multiples in the data.

Finally, we notice the similarities between the pseudophysical parts of SRI and the ISS in the numerical examples presented above. This implies that there might be further links between the two representations of scattered fields, for example, an implicit relationship between the other terms in SRI and higher order contributions in the ISS. Part of our future research will explore this relationship, in the hope that we may gain new insight into each of the two methods by taking information from the other.

CONCLUSIONS

We summarize the derivation of the ISS equation for estimating internal multiples and present a second derivation of the same equation starting from SRI. For the first time, this provides an explicit relationship between the two domains of inverse scattering and interferometry. The use of pseudophysical energy for internal-multiple estimation in both methods is highlighted and compared. Using the interferometric perspective, we propose an alternative representation for internal-multiple prediction that takes advantage of convolution and correlation operations in the frequency domain. It allows us to compute internal multiples more efficiently, which is confirmed by a comparison of both representations applied to a synthetic single-trace example and a synthetic common-shot gather.

ACKNOWLEDGMENTS

We thank the Edinburgh Interferometry Project sponsors (ConocoPhillips, Schlumberger Cambridge Research, Statoil, and Total) for supporting this research and granting us permission to publish. Furthermore, we wish to thank the editor J. van der Neut, A. Malcolm, J. Sheiman, and an anonymous reviewer for their profound and constructive revisions of our work.

REFERENCES

Araujo, F. V., A. B. Weglein, P. M. Carvalho, and R. H. Stolt, 1994, Inverse scattering series for multiple attenuation: An example with surface and internal multiples: 64th Annual International Meeting, SEG, Expanded Abstracts, 1039–1041.

Behura, J., and F. Forghani, 2012, A practical approach to prediction of internal multiples and ghosts: 82nd Annual International Meeting, SEG, Expanded Abstracts, doi: 10.1190/segam2012-1269.1.

Berkhout, A. J., and D. J. Verschuur, 1997, Estimation of multiple scattering by iterative inversion, Part I: Theoretical considerations: Geophysics, **62**, 1586–1595, doi: 10.1190/1.1444261.

Born, M., and E. Wolf, 1999, Principles of optics — Electromagnetic theory of propagation, interference and diffraction of light (7th ed.): Cambridge University Press.

Curtis, A., Y. Behr, E. Entwistle, E. Galetti, J. Townend, and S. Bannister, 2012, The benefit of hindsight in observational science: Retrospective seismological observations: Earth and Planetary Science Letters, **345–348**, 212–220, doi: 10.1016/j.epsl.2012.06.008.

Curtis, A., and D. Halliday, 2010, Source-receiver wavefield interferometry: Physical Review E, **81**, 046601, doi: 10.1103/PhysRevE.81.046601.

Curtis, A., H. Nicolson, D. Halliday, J. Trampert, and B. Baptie, 2009, Virtual seismometers in the subsurface of the Earth from seismic interferometry: Nature Geoscience, **2**, 700–704, doi: 10.1038/ngeo615.

Duguid, C., D. Halliday, and A. Curtis, 2011, Source-receiver interferometry for seismic wavefield construction and ground roll removal: The Leading Edge, **30**, 838–843, doi: 10.1190/1.3626489.

Entwistle, E., A. Curtis, E. Galetti, B. Baptie, and G. A. Meles, 2015, Constructing new seismograms from old earthquakes: Retrospective seismology at multiple length scales: Journal of Geophysical Research: Solid Earth, **120**, 2466–2490.

Fleury, C., 2013, Increasing illumination and sensitivity of reverse-time migration with internal multiples: Geophysical Prospecting, **61**, 891–906, doi: 10.1111/1365-2478.12041.

Fleury, C., and I. Vasconcelos, 2012, Imaging condition for nonlinear scattering-based imaging: Estimate of power loss in scattering: Geophysics, **77**, no. 1, S1–S18, doi: 10.1190/geo2011-0135.1.

Halliday, D., and A. Curtis, 2010, An interferometric theory of source-receiver scattering and imaging: Geophysics, **75**, no. 6, SA95–SA103, doi: 10.1190/1.3486453.

Hampson, D., 1986, Inverse velocity stacking for multiple elimination: Canadian Journal of Exploration Geophysicists, **22**, 44–55.

Hong, T., and W. Menke, 2006, Tomographic investigation of the wear along the San Jacinto fault, southern California: Physics of the Earth Planetary Interiors, **155**, 236–248, doi: 10.1016/j.pepi.2005.12.005.

Hung, B., and M. Wang, 2012, Internal demultiple methodology without identifying the multiple generators: 82nd Annual International Meeting, SEG, Expanded Abstracts, doi: 10.1190/segam2012-0549.1.

Jakubowicz, H., 1998, Wave equation prediction and removal of interbed multiples: 68th Annual International Meeting, SEG, Expanded Abstracts, 1527–1530.

Jiang, S., J. Sheng, J. Yu, G. T. Schuster, and B. E. Hornby, 2007, Migration methods for imaging different-order multiples: Geophysical Prospecting, **55**, 1–19, doi: 10.1111/j.1365-2478.2006.00598.x.

Kaplan, S., K. A. Innanen, E. Otnes, and A. B. Weglein, 2005, Internal multiple attenuation code-development and implementation: Mission-Oriented Seismic Research Program (M-OSRP) Annual Report, 83–102.

Keydar, S., E. Landa, B. Gurevich, and B. Gelchinsky, 1997, Multiple prediction using wavefront characteristics of primary reflections: 59th Annual International Conference and Exhibition, EAGE, Extended Abstracts, A016.

King, S., and A. Curtis, 2012, Suppressing nonphysical reflections in Green's function estimates using source-receiver interferometry: Geophysics, **77**, no. 1, Q15–Q25, doi: 10.1190/geo2011-0300.1.

Liang, H., C. Ma, and A. B. Weglein, 2013, General theory for accommodating primaries and multiples in internal multiple algorithm: Analysis and numerical tests: 83rd Annual International Meeting, SEG, Expanded Abstracts, 4178–4183.

Lippmann, B. A., and J. Schwinger, 1950, Variational principles for scattering processes: Physical Review, **79**, 469–480, doi: 10.1103/PhysRev.79.469.

Löer, K., G. A. Meles, and A. Curtis, 2015, Automatic identification of multiply diffracted waves and their ordered scattering paths: Journal of the Acoustical Society of America, **137**, 1834–1845, doi: 10.1121/1.4906839.

Löer, K., G. A. Meles, A. Curtis, and I. Vasconcelos, 2014, Diffracted and pseudo-physical waves from spatially-limited arrays using source-receiver interferometry (SRI): Geophysical Journal International, **196**, 1043–1059, doi: 10.1093/gji/ggt435.

Ma, C., and A. B. Weglein, 2014, Including higher-order inverse scattering series terms to address a serious shortcoming/problem of the internal-multiple attenuator: Exemplifying the problem and its resolution: 84th Annual International Meeting, SEG, Expanded Abstracts, 4124–4129.

Malcolm, A. E., and M. V. de Hoop, 2005, A method for inverse scattering based on the generalized Bremmer coupling series: Inverse Problems, **21**, 1137–1167, doi: 10.1088/0266-5611/21/3/021.

Malcolm, A. E., M. V. de Hoop, and H. Calandra, 2007, Identification of image artifacts due to internal multiples: Geophysics, **72**, no. 2, S123–S132, doi: 10.1190/1.2434780.

Malcolm, A. E., B. Ursin, and M. V. de Hoop, 2009, Seismic imaging and illumination with internal multiples: Geophysical Journal International, **176**, 847–864, doi: 10.1111/j.1365-246X.2008.03992.x.

Meles, G. A., and A. Curtis, 2013, Physical and non-physical energy in scattered wave source-receiver interferometry: Journal of the Acoustical Society of America, **133**, 3790–3801, doi: 10.1121/1.4802825.

Meles, G. A., and A. Curtis, 2014, Finger-printing ordered diffractions in multiply-diffracted waves: Geophysical Journal International, **198**, 1701–1713, doi: 10.1093/gji/ggu195.

Meles, G. A., K. Löer, M. Ravasi, A. Curtis, and C. A. da Costa Filho, 2014, Internal multiple prediction and removal using Marchenko autofocusing and seismic interferometry: Geophysics, **80**, no. 1, A7–A11, doi: 10.1190/geo2014-0408.1.

Poliannikov, O., 2011, Retrieving reflections by source-receiver interferometry: Geophysics, **76**, no. 1, SA1–SA8.

Ramírez, A. C., and A. B. Weglein, 2005, An inverse scattering internal multiple elimination method: Beyond attenuation, a new algorithm and initial tests: 75th Annual International Meeting, SEG, Expanded Abstracts, 2115–2118.

Ravasi, M., and A. Curtis, 2013, Nonlinear scattering based imaging in elastic media: Theory, theorems and imaging conditions: Geophysics, **78**, no. 3, S137–S155, doi: 10.1190/geo2012-0286.1.

Ravasi, M., I. Vasconcelos, and A. Curtis, 2014, Beyond conventional migration: Non-linear elastic subsalt imaging with transmissions and two-sided illumination: Geophysical Journal International Geophysics, **198**, 1173–1185, doi: 10.1093/gji/ggu192.

Snieder, R., 2004, Extracting the Green's function from the correlation of coda waves: A derivation based on stationary phase: Physical Review E, **69**, 046610, doi: 10.1103/PhysRevE.69.046610.

Snieder, R., K. van Wijk, M. Haney, and R. Calvert, 2008, Cancellation of spurious arrivals in Green's function extraction and the generalized optical theorem: Physical Review E, **78**, 036606.1–036606.8, doi: 10.1103/PhysRevE.78.036606.

ten Kroode, F., 2002, Prediction of internal multiples: Wave Motion, **35**, 315–338, doi: 10.1016/S0165-2125(01)00109-3.

Van Manen, D.-J., A. Curtis, and J. O. A. Robertsson, 2006, Interferometric modeling of wave propagation in inhomogeneous elastic media using time reversal and reciprocity: Geophysics, **71**, no. 4, SI47–SI60, doi: 10.1190/1.2213218.

Van Manen, D.-J., J. O. A. Robertsson, and A. Curtis, 2005, Modeling of wave propagation in inhomogeneous media: Physical Review Letters, **94**, 164301, doi: 10.1103/PhysRevLett.94.164301.

Vasconcelos, I., P. Sava, and H. Douma, 2010, Nonlinear extended images via image-domain interferometry: Geophysics, **75**, no. 6, SA105–SA115, doi: 10.1190/1.3494083.

Vasconcelos, I., and R. Snieder, 2008, Interferometry by deconvolution, Part 1 — Theory for acoustic waves and numerical examples: Geophysics, **73**, no. 3, S115–S128, doi: 10.1190/1.2904554.

Verschuur, D. J., 2013, Seismic multiple removal techniques — Past, present and future (revised ed.): EAGE Publications B.V.

Verschuur, D. J., A. J. Berkhout, and K. Wapenaar, 1992, Adaptive surface-related multiple elimination: Geophysics, **57**, 1166–1177, doi: 10.1190/1.1443330.

Wapenaar, K., 2004, Retrieving the elastodynamic Green's function of an arbitrary inhomogeneous medium by cross correlation: Physical Review Letters, **93**, 254301, doi: 10.1103/PhysRevLett.93.254301.

Wapenaar, K., and J. Fokkema, 2006, Green's function representation for seismic interferometry: Geophysics, **71**, no. 6, SI33–SI46, doi: 10.1190/1.2213955.

Weglein, A. B., F. V. Araújo, P. M. Carvalho, R. H. Stolt, K. H. Matson, R. T. Coates, D. Corrigan, D. J. Foster, S. A. Shaw, and H. Zhang, 2003, Inverse scattering series and seismic exploration: Inverse Problems, **19**, R27–R83, doi: 10.1088/0266-5611/19/6/R01.

Weglein, A. B., F. A. Gasparotto, P. M. Carvalho, and R. H. Stolt, 1997, An inverse-scattering series method for attenuating multiples in seismic reflection data: Geophysics, **62**, 1975–1989, doi: 10.1190/1.1444298.

Downloaded 04/08/16 to 129.215.249.201. Redistribution subject to SEG license or copyright; see Terms of Use at http://library.seg.org/